Using Hyperspectral Imaging to Quantify Phototrophic Biofilms on Granite

A. Ramil[1], D. Vázquez-Nion[2], J. S. Pozo-Antonio[3] *, P. Sanmartín[2], and B. Prieto[2]

[1]*Laboratorio de Aplicacións Industriais do Láser, Centro de Investigacions Tecnoloxicas (CIT), Departamento de Enxeñaría Naval e Industrial, Escola Politécnica Superior, Universidade de A Coruña (UDC), Campus Ferrol, 15403-Ferrol, Spain*
[2]*Departamento de Edafoloxía e Química Agrícola. Facultade de Farmacia. Universidade de Santiago de Compostela, 15782 - Santiago de Compostela, Spain*
[3]*Departamento de Enxeñaría dos Recursos Naturais e Medio Ambiente, Escola de Enxeñaría de Minas e Enerxía, Universidade de Vigo, 36310-Vigo, Spain*

ABSTRACT. This paper reports a non-invasive method for in situ biofilm quantification based on the use of hyperspectral imaging to analyze a chromatically and texturally heterogeneous substrate as granite colonized by green algae and cyanobacteria. Biofilm-forming microorganisms were inoculated on granite blocks and incubated under laboratory conditions for 21 days. The intensity of the green stains formed on the granite surfaces differed depending on the initial concentration of microorganisms used. A biofilm quantification (BQ) index was computed to determine the level of colonization on the surfaces. The index was obtained by comparing the quotient of the reflectance of the green (G) and red (R) bands of each pixel of the hyperimage against a threshold value, f_{th}. The optimal value of the threshold was determined by examining the linear correlation between the BQ index and the chlorophyll a extracted. The BQ results were then compared with the F_0 and ΔE^*_{ab} parameters yielded by colour spectrophotometry and PAM fluorometry techniques and used as reference methodologies to quantify greening on stone surfaces. The BQ index showed a high level of consistency with all of the other parameters; it was linearly correlated with the chlorophyll a concentration, F_0 and ΔE^*_{ab}, with high coefficients of determination ($r^2 > 0.92$) for the range from 1.87 to 5.69 µg chl a.cm^{-2}. The strength of the BQ index lies in its double use as a biomarker of quantity and percentage cover, as well as its good performance under different conditions, ranging from initial phototrophic colonization and thin (young) biofilms covering 21.19% of the surface to profuse biological colonization covering 67.36% of the surface. Moreover, the proposed BQ index may be able to be used with other types of rock with less heterogeneous surfaces than granite.

Keywords: biofilms, chlorophyll fluorescence, colour spectrophotometry, hyperspectral imaging, non-invasive technique

1. Introduction

Stone monuments, like most exposed surfaces, are prone to being colonized by living organisms. Microorganisms such as actinobacteria, cyanobacteria, algae and fungi form sub-aerial biofilms (SABs), defined as microbial communities that develop on solid mineral surfaces exposed to the atmosphere (Gorbushina, 2007). In regions with oceanic climate, such as Western Europe and parts of central Mexico and the Pacific Northwest of the USA, characterized by warm summers and cool winters with high atmospheric humidity, sub-aerial green biofilms form on exposed stone surfaces ('greening') (Crispim and Gaylarde, 2005; Scheerer et al., 2009; Cutler et al., 2013). The colour of biofilms is caused by the chlorophyll contained in algae and cyanobacteria, the main components of the films. Biofilms cause aesthetic damage and obvious discolouration of the substrate. However, there is some controversy as to the impact of greening on the physical integrity of stone. Although classic studies describe its role in biodeterioration (Ortega-Calvo et al., 1991a, b), biofilms are also considered to have a bioprotective role (Ramirez et al., 2010; Cutler et al., 2013). Sub-aerial green biofilms are becoming increasingly important as ecological models, providing new means of developing and implementing ecological principles (Villa et al., 2016) and of addressing environmental problems, e.g., remediation of the visual impact generated by opencast mining (Prieto et al., 2005).

For quantification of sub-aerial green biofilms, nondisruptive and portable techniques (which can be used on site) are preferred. Colour spectrophotometry and pulse amplitude modulated (PAM) fluorometry have been used on stone building materials for this purpose in recent years, with good results (Eggert et al., 2006; Sanmartín et al., 2012; von Werder and Venzmer, 2013; Eyssautier-Chuine et al., 2015; Vázquez-Nion et al., 2018). Colour measurements made with a portable spectrophotometer and represented in the CIELAB colour space (Colorimetry CIE Central Bureau, 1986), in which the main parameter is the total colour difference (ΔE^*_{ab}), have several advantages over other methods. The main advantages, apart from being a non-disruptive and portable technique, are its

relatively low cost and ease of application, enabling unskilled operators with minimal training to perform the measurements. Results are obtained immediately, with little data processing required, and the technique enables early detection of biological colonization, even before it is visible to the human eye (Prieto et al., 2002, 2005; Sanmartín et al., 2012).

PAM fluorometry enables estimation of 'greening' on the basis of F_0 values, i.e., fluorescence yield after dark adaptation (when the photosynthetic apparatus is in a quiescent state and all photosystem II (PSII) reaction centres fully open). The method is based on the assumed mathematical relationship between the concentration of chlorophyll *a* (a biomarker used to quantify phototrophic biomass) and the mean fluorescence yield of dark-adapted cells measured under laboratory conditions, as reported by Eggert et al. (2006) and Vázquez-Nion et al. (2018). The model developed by Eggert et al. (2006) is valid for a pooled isolate of aeroterrestrial green algae and for chlorophyll *a* concentrations ranging between 3.5 and 20 mg chl *a* m^{-2}. The quadratic model of Vázquez-Nion et al. (2018) is valid for a multi-species phototrophic culture (composed by bryophyta, charophyta, chlorophyta and cyanobacteria) up to 70 mg chl *a* m^{-2}. Other authors have recently validated the use of F_0 for estimating the abundance of algal biomass in outdoor weathering tests (Gladis and Schumann, 2011; von Werder and Venzmer, 2013), while also confirming that, like colour spectrophotometry, the level of detection provided by F_0 is lower than yielded by visual inspection. However, F_0 and chlorophyll *a* will never be fully correlated, because the total amount of chlorophyll does not only consist of the amount of chlorophyll per photosystem II centre (quantified by F_0) but also includes the fluorescence of PSI-associated chlorophyll *a*. Moreover, the presence of cyanobacteria in algal biofilms would also further disrupt the correlation between the fluorescence yield and the chlorophyll *a* content (von Werder and Venzmer, 2013).

Limitations of the techniques discussed include the difficulty in their application to large areas of monuments or façades because of the small measuring area of the devices, thus hindering evaluation of the spatial distribution of the phototrophic colonization. Colour spectrophotometers have a circular target area of no more than 60 mm in diameter and PAM fluorometers have optical fibres of diameter 1 ~ 8 mm. This not only implies the need for multiple measurements but also the use of scaffolding (or similar) in order to reach high surfaces. The field of measurement of the devices is limited and moreover, the measurement of chromatically and texturally heterogeneous surfaces, such as granite, therefore produces unrealistic colour values due to integration of the colours captured. In addition to the possible difficulties in reaching the target object with the colour measuring and PAM instruments, the devices also require annual or biannual calibration (costing around 1000 EUR).

These limitations favour the use of digital cameras in which the field of view is not limited to a small area, contact with the target object is not required and, moreover, simultaneous encoding of each point of the surface is possible,
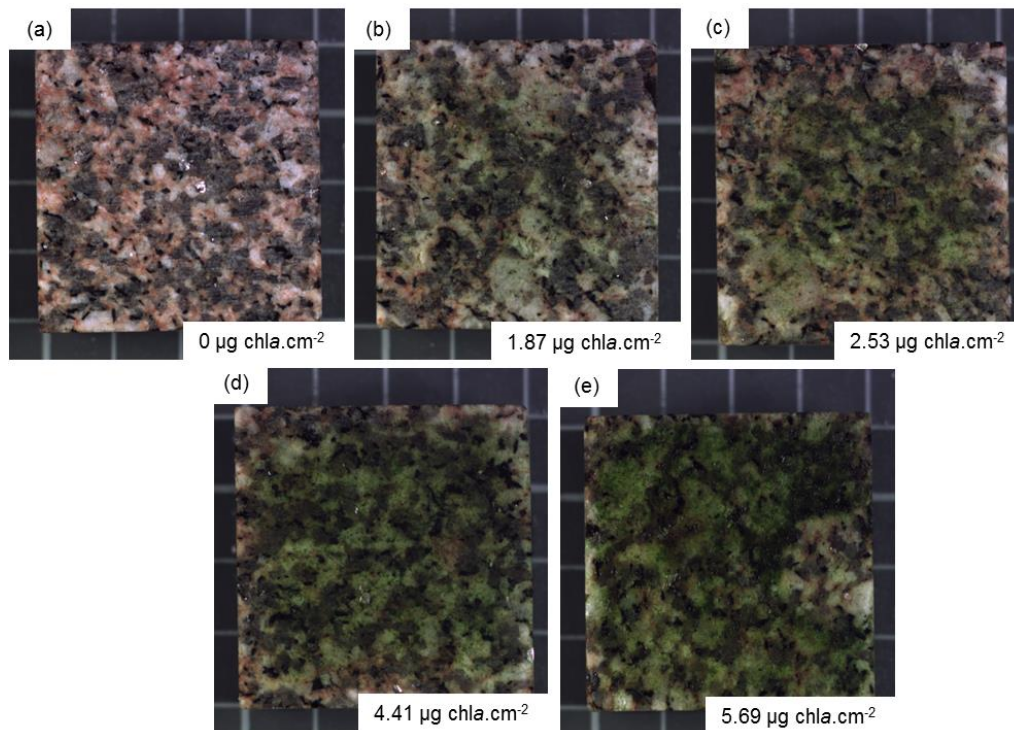

Figure 1. Digital photographs of the surfaces of the granite blocks (4 cm × 4 cm) 21 days after inoculation. The chlorophyll *a* content is shown in each case. (a) uninoculated block; (b), (c), (d) and (e) blocks inoculated with microorganism cultures of concentrations 0.05, 0.10, 0.15, and 0.20 mg·cm^{-2} (dry weight biomass), respectively.

which is advantageous for detecting biological remains between the grains on stone walls.

Hyperspectral cameras, initially developed for remote sensing applications, incorporate conventional digital imaging and spectroscopy thus enabling the simultaneous delivery of spatial and spectral information (Goetz, 2009; Eismann, 2012; van der Meer et al., 2012). They can be used to characterize large and/or heterogeneous surfaces, revealing the distribution, percentage of components and surface characteristics (Gowen et al., 2015; López et al., 2017). Hyperspectral images are suitable for identifying granite-forming minerals via a robust algorithm (artificial neural network) in laser cleaning (López et al., 2017). In order to produce a spatial map of the distribution of chlorophyll *a* on intertidal sediment surfaces on the basis of reflectance measurements, Carrère et al. (2004) used three different approaches (band-ratio, scaled-band depth and scaled-band area) to estimate the concentration of chlorophyll *a*. These authors considered the relationship between the reflectance at a wavelength at which chlorophyll *a* typically absorbs (673 nm) and the reflectance at a wavelength where absorption is not attributable to chlorophyll *a* (720 nm). The scaled-band area method provided slight better results than the other two approaches. Similarly, Chennu et al. (2013) used hyperspectral imaging to map the distribution of microphytobenthos biomass in intertidal sediments, with a high spatial resolution over areas of 1×1 m. The aforementioned authors stabilised the relationship between the reflectance at the typical wavelength at which chlorophyll *a* absorbs (673 nm) and the reflectance at the NIR range (720 ~ 800 nm) without any absorption attributable to chlorophyll *a*, following Carrère et al. (2004). Hyperspectral imaging techniques have also been used to monitor the laser cleaning of biotic (biofilms-forming cyanobacteria, algae and fungi and lichenic crusts) and abiotic (sulphated black crust and graffiti paints) deposits on granite (Pozo-Antonio et al., 2015, 2016 a,b). However, despite its potential usefulness, hyperspectral imaging has not yet been used to quantify phototrophic biofilm covering chromatically and texturally heterogeneous stone substrates, such as granite.

The aim of this study was to demonstrate the potential use of hyperspectral imaging to compute a reliable index for estimating biofilm development on granite. For this purpose, a laboratory-scale hyperspectral imaging system was used to determine the spatial distribution and the level of phototrophic colonization of granite samples, 21 days after the samples were inoculated with different quantities of phototrophic microorganisms. Reflectance was measured in the 450 ~ 700 nm region of the visible spectrum. Due to the heterogeneity of the granite substrate texture, we opted to use a procedure to classify the pixels of the hyperspectral image. Thus, we calculated a biological colonization index (*BQ*, %) from the quotient of the reflectance between the green (*G*) and red (*R*) bands, f_{GR}, with a threshold value, f_{th}, considered to indicate the presence of algae. The optimal value of the threshold was determined by searching for the closest correlation between *BQ* (percentage of pixels with $f_{GR} > f_{th}$) and the chlorophyll *a* content extracted. The *BQ* was also correlated with the values of ΔE^*_{ab} (colour spectrophotometry) and F_0 (PAM fluorometry), in order to identify the reliability of the proposed index when applied to granite.

2. Materials and Methods

2.1. Sample Preparation

Granite is a major construction material in European historical buildings and monuments (Vicente et al., 1996). The type of granite selected for the experiment was the commercially available Silvestre AM (hereinafter SAM), a medium-grained allotriomorphic monzogranite, containing plagioclase (31%), quartz (30%), K-feldspar (24%), muscovite (8%) and biotite (6%) as main minerals. The open porosity (3.66%) and bulk density (2.55 g·cm⁻³) were determined following EN 1936 ~ 1999, (1999). This granite is white with some ochre spots due to biotite weathering and is very similar to that used in most of the cultural heritage buildings and monuments in the NW Iberian Peninsula, e.g., the Cathedral of Santiago de Compostela.

Five blocks (4cm × 4cm × 2cm) with disc-cutting finish were cut and sterilized in autoclave before the start of the experiments. The upper surface of each granite block (16 cm²) was inoculated in a laminar flow cabinet with a multi-species culture derived from a natural biofilm growing on a granite wall of the San Martín Pinario Monastery (Santiago de Compostela, Spain) and composed of green algae (mainly *Chlorella* sp., *Stichococcus bacillaris, Bracteacoccus* sp. and *Chlamydomonas* sp.) and cyanobacteria (*Aphanocapsa* sp. and *Leptolyngbya cebennensis*) (Vázquez-Nion et al., 2016). Four of the blocks were inoculated with different concentrations of microorganisms (0.05, 0.10, 0.15, and 0.20 mg·cm⁻² dry weight biomass), and one (uninoculated) block was reserved as a reference sample. The granite blocks were incubated in a climatic chamber under stationary conditions of 23ºC, 95% *RH* and 12 h of light (31 μmol photons m⁻² s⁻¹) / dark photo-
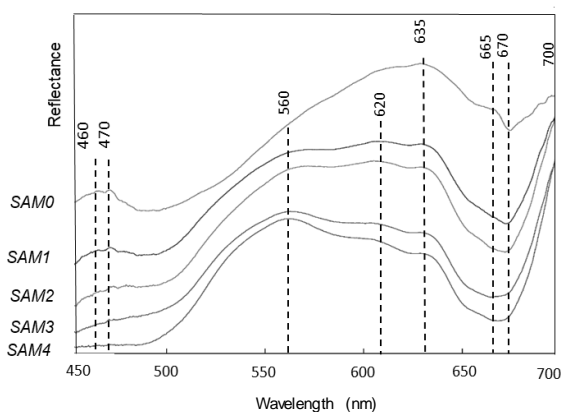

Figure 2. Reflectance spectra for the reference (uninoculated) granite block (SAM0), and blocks inoculated with dry weight biomass concentrations of 0.05 (SAM 1), 0.10 (SAM2), 0.15 (SAM3), and 0.20 mg·cm⁻² (SAM4).

Table 1. Colorimetric Differences (ΔL^*, Δa^*, and Δb^*) and Global Colour Change (ΔE^*_{ab}) for the Surfaces of the Granite Blocks Inoculated with the Different Concentrations of Microorganisms

Biomass concentration (μg chl a.cm^{-2})	ΔL^*	Δa^*	Δb^*	ΔE^*_{ab}
1.87	-7.29	-4.69	6.01	10.55
2.53	-11.04	-7.72	7.73	15.53
4.41	-12.82	-9.13	11.63	19.56
5.69	-16.29	-9.99	12.01	22.57
Predictive equation biomass (μg chl a.cm^{-2})	-0.3442ΔL^* - 0.3647	-0.5153Δa^* - 0.3488	0.4382Δb^*- 0.376	0.2417ΔE^*_{ab} - 0.3973
R^2	> 0.90	> 0.90	> 0.90	> 0.90

* Colour differences were computed relative to the colour of the reference surface; thus, the greater the difference, the greater the amount of biofilm on the surface.

period for twenty-one days in order to induce biofilm formation.

2.2. Quantification of Phototrophic Biomass

In order to evaluate the suitability of the non-invasive hyperspectral imaging technique to develop a reliable biofilm quantification (*BQ*) index, other invasive and non-invasive analytical techniques were used to quantify the phototrophic biomass on the stones, i.e. chemical extraction of chlorophyll *a*, and colour spectrophotometry and PAM chlorophyll fluorescence.

2.2.1. Chemical Extraction of Chlorophyll *a* (chl *a*)

In order to quantify the phototrophic biomass on each granitic block after inoculation and incubation for twenty-one days, chlorophyll *a* was extracted following the protocol developed by Fernandez-Silva et al. (2011) for biofilms colonizing rocks. The extracts were measured in a UV–Visible spectrophotometer (UVIKON XS, Bio-Tek), and the equation proposed by Wellburn (1994) was used to calculate the concentration of chlorophyll *a*, expressed as μg chl a.cm^{-2} of surface area.

2.2.2. Colour Spectrophotometry

The surface colour of each granitic block was measured before inoculation and after development of the biofilm, with a portable spectrophotometer (Konica Minolta CM-700d) equipped with CM-S100w (SpectraMagicTM NX) software, as described by Prieto et al. (2010 a,b). Measurements consisted of a total of 9 readings randomly taken in different areas of each block under the following conditions: illuminant D65, observer angle 2, specular component included (SCI) mode, 10 mm diameter target area, integration time 1 second, and a spectral range 360 ~ 740nm with a spectral resolution of 10 nm. Colour measurements were analysed using the CIELAB colour system (Colorimetry CIE Central Bureau, 1986). This system is widely accepted by both the scientific community and industry because it provides the most 'perceptually uni-

form' (i.e. a change of the same amount in a colour value should produce a change of about the same visual importance) measurement of the colour spaces (Berns, 2000; Völz, 2001). The CIELAB system has also been used by conservation scientists to detect the growth of microorganisms on granite rocks (Sanmartín et al., 2012; Vázquez-Nion et al., 2018). The colour coordinates measured were the three scalar parameters: *L**, lightness which varies from 0 (absolute black) to 100 (absolute white); *a**, related to colour changes in the red – green range (+*a**: red and -*a**: green); and *b**, associated with changes in the yellow – blue range (+*b**: yellow and -*b**: blue). In order to evaluate phototrophic biomass, colour data were processed as partial colour differences (ΔL^*, Δa^*, and Δb^*) and global colour change (ΔE^*_{ab}) between the block before inoculation and 21 days later. This enables quantification of the colour change caused by phototrophic organisms, which is related to phototrophic biomass. Thus, colour differences were calculated as follows:

$$\Delta L^* = L^*_x - L^*_0; \tag{1}$$

$$\Delta a^* = a^*_x - a^*_0; \tag{2}$$

$$\Delta b^* = b^*_x - b^*_0; \tag{3}$$

$$\Delta E^*_{ab} = [(\Delta L^*)^2 + (\Delta a^*)^2 + (\Delta b^*)^2]^{1/2}; \tag{4}$$

the subscript *x* denotes the colour parameter of a block inoculated with *x* inoculum concentration after 21 days of incubation and the subscript 0 denotes the colour parameter of the same block before inoculation. Uninoculated blocks were used as negative controls.

2.2.3. Pulse Amplitude Modulated (PAM) Fluorometry

In vivo chlorophyll *a* (chl *a*) fluorescence was measured with a PHYTO-PAM fluorometer (Heinz Walz GmbH, Effeltrich, Germany) equipped with a fibre optics emitter-detector unit PHYTO-EDF. Measurements were carried out with a perspex cylinder (4 mm diameter) in direct contact with the surface of the wet-inoculated granitic blocks, by taking 16 readings in randomly selected areas of each sample (Vázquez-

Nion et al., 2018). The blocks were kept in darkness for at least 20 min prior to the measurements. The measuring light applied corresponds to an integrated intensity of 0.15 µmol photon m^{-2} s^{-1}, the actinic effect of which could be neglected, and gain was set to a value of 14. The fluorescence parameter recorder used in this study was F_0, the minimal fluorescence signal in dark-adapted cells, measured at four wavelengths of 665, 645, 520, and 470 nm. No background signal was detected in uninoculated blocks.

2.2.4. Hyperspectral Imaging Technique

The photographic equipment used consisted of a Pulnix TM-1327 GE CCD sensor (1040 rows, 1392 columns) with a 10 mm focal length objective lens; an ImSpector V10 spectrograph with a spectral range of 400 ~ 1000 nm was fitted between the sensor and the lens. The spectral camera captured images of a linear array of 1392 pixels, with the light spec-

trum at each pixel spread into 1040 bands in the range of 400 ~ 1000 nm. The resulting spectral resolution of camera and spectrograph is 4.55 nm. Optimal measurement conditions of the system are obtained in the spectral visible range 450 ~ 700 nm. The sample was placed on a motorized 3D translation stage (Newport ILS-CC), externally controlled by a motion controller (Newport MM4006). The stage was able to be moved vertically, so that the camera scanned the surface, line by line, in order to obtain an image at each of the 1040 bands. The light source was an incandescent lamp (Schott DCR® III) with rectangular head of length 51 mm and width 0.89 mm. A cylindrical lens placed in front of the head focused the light so that the illuminated area was similar to an ellipse with major axis 15 cm and minor axis 1 cm.

The pixel/mm ratio was estimated as a function of the distance between the sample and the camera distance and, combined with the vertical displacement of the object, al-
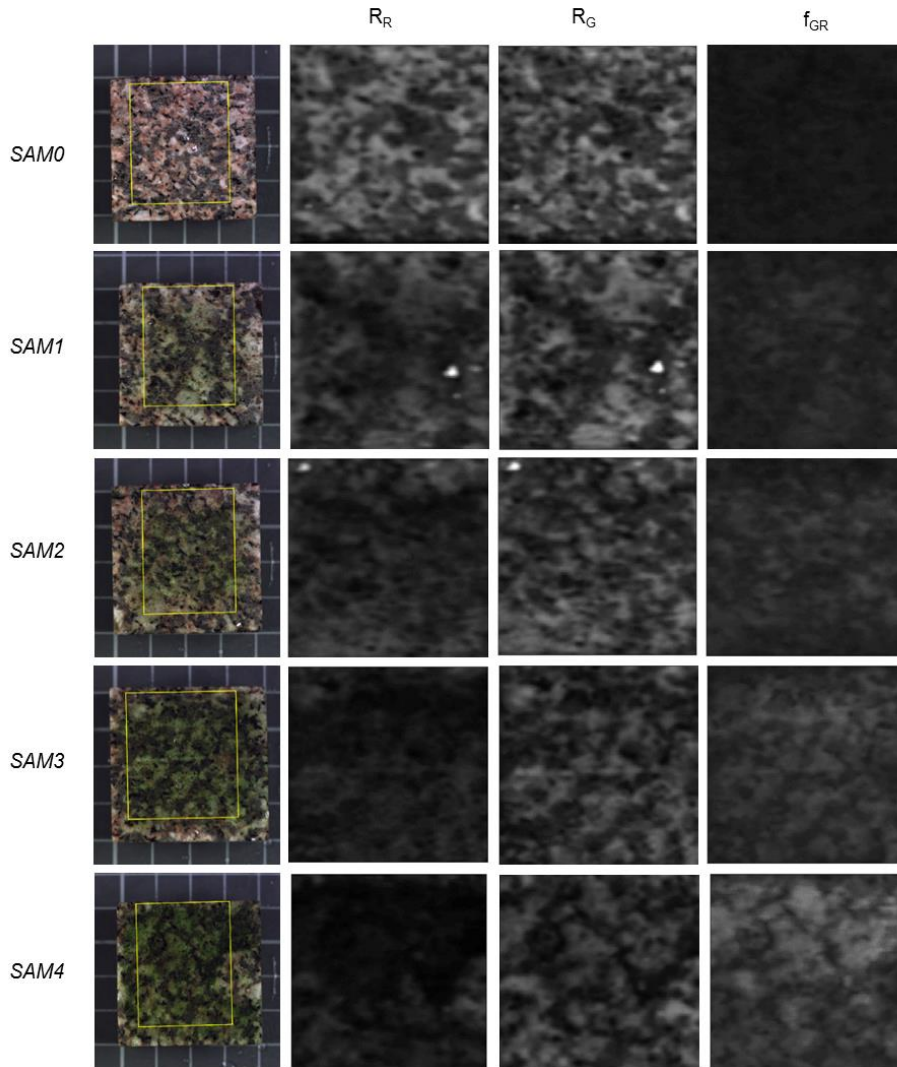

Figure 3. For each row, reference surface without inoculum (SAM0), and inoculated with dry weight biomass 0.05 (SAM1), 0.10 (SAM2), 0.15 (SAM3), and 0.20 mg·cm^{-2} (SAM4). The columns show the digital photographs, images of the reflectance of the red (R_R) and green (R_G) bands and the map of the quotient f_{GR}.

lowed us to accurately assign an image to each point on the surface. In order to obtain the reflectance spectra for each pixel, the spectral data were corrected to the dark noise and normalized to an ideal white (maximum reflectivity):

$$R(\lambda) = \frac{I_G(\lambda) - I_{BG}}{I_W(\lambda) - I_{BG}} \tag{5}$$

where I is the intensity of each pixel of the granite (I_G), of the white reference (I_W) and background (I_{BG}).

Once the reflectance spectra were obtained, an index was computed for biofilm quantification (BQ index) and determination of its spatial distribution. As the algorithm used to calculate this index was based on the samples obtained, its development will be discussed in section *3. Results and Discussions.*

2.3. Statistical Correlations

Once the measurements and the required computations were performed, the equation used to predict phototrophic biomass yield and also the coefficient of determination (r^2) between the results obtained for each parameter and the biomass concentration determined by chemical extraction of chlorophyll *a* (chl *a*), were processed using Matlab package *Statistics and Machine Learning Toolbox™*.

Moreover, the coefficient of determination, r^2 and *p*- values for the relationships between the selected parameters computed with *BQ* index were determined in order to evaluate the reliability of the hyperspectral imaging technique for quantifying the biofilm.

3. Results and Discussions

The epilithic phototrophic biofilms induced on the granitic blocks in the laboratory served to emulate the presence of green fouling ("greening") due to the chlorophyll *a* contained
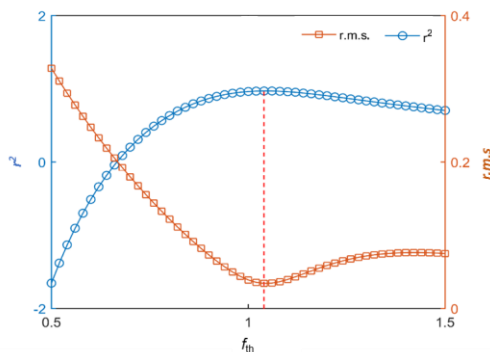

Figure 4. Values of the correlation coefficient, r^2, and the root mean square error (*r.m.s.*) for the linear fit between BQ and the amount of chlorophyll *a* as a function of fth. The highest r^2 value and the lowest *r.m.s.* correspond to f_{th} = 1.04 (indicated by a dotted line).

in green algal and cyanobacterial cells. The biofilm was macroscopically visible on all inoculated blocks and the extent of biological cover and the amount of biomass, expressed as concentration of chlorophyll *a*, were related to the inoculum concentration (Figure 1).

3.1. Colour Spectrophotometry

Table 1 shows the values of the partial colour differences (ΔL^*, Δa^* and Δb^*) and the total colour difference or global colour change (ΔE^*_{ab}) of the inoculated blocks relative to the uninoculated block. The L^* and a^* values decreased and the b^* increased both significantly, with the biomass concentration, as for all inoculum concentrations, ΔL^*, Δa^*, Δb^* and global colour changes ΔE^*_{ab} exceeded the widely perceptible threshold colour of 3 CIELAB units (Berns, 2000; Prieto et al., 2010 a,b). The colour surface thus became darker and exhibited a stronger yellow-greenish colour as the amount of microorganisms on the surface increased. The b^* varied more than a^* for the same amount of biomass (Table 1). This is consistent with the findings of previous studies on monitoring greening growth on façades, indicating parameter b^* (rather than a^*) as a useful indicator for monitoring the earliest colonization on surfaces of quartz (Prieto et al., 2005), concrete (De Muynck et al., 2009) and granite (Sanmartín et al., 2012). In addition, taking into account the magnitude of the colour change caused by colonization, the lightness parameter (L^*) varied most widely and thus contributed the most to the global colour change (ΔE^*_{ab}). The analysis of ΔL^* values has already proved useful for quantifying changes in pigment concentrations associated with the phototrophic biomass yield (Sanmartín et al., 2010) and the physiological state of the microorganisms (Sanmartín et al., 2011).

Table 1 also shows the mathematical relationship between the colour differences and the biomass achieved, expressed as µg chl $a \cdot cm^{-2}$, at the end of the incubation period. The colorimetric differences increased as biomass concentration increased with coefficient of determination (r^2) values higher than 0.90. As all the matches between biomass and colour parameters were large and similar, ΔE^*_{ab} was selected for comparison with the *BQ* index, because it is the main parameter in the CIELAB colour space and the most commonly used in different studies for quantifying phototrophic biomass.

3.2. *PAM* Fluorometry

Fluorescence yield after dark adaptation, F_0 value, of the four measurement channels at 470, 520, 645, and 665 nm was recorded (Table 2). In the four cases, as for the colour measurements, F_0 values increased with the concentration of microorganisms on the granite surface. The fluorescence F_0 at 470, 520, 645, and 665 nm was linearly related to the biomass, expressed as µg chl $a \cdot cm^{-2}$, and the coefficient of determination r^2 was very similar and higher than 0.90 in all cases (Table 2). The F_0 intensity was higher at 665 nm, while the intensity of F_0 at 470 and 520 and 645 nm was similar and relatively low.   We thus chose F_0 at 665 nm for comparison

Table 2. F_0 (relative units), the Minimal Fluorescence Signal of Dark Adapted Cells, at 470, 520, 645 and 665 nm, for Each Inoculated Surface with Different Concentrations by Means of the PHYTO-PAM Fluorometer

Biomass concentration (μg chl *a*. cm^{-2})	F_0 at 470 nm	F_0 at 520 nm	F_0 at 645 nm	F_0 at 665 nm
1.87	73.88	68.63	171.63	174.75
2.53	125.44	126.50	300.44	297.38
4.41	161.31	164.63	360.88	354.19
5.69	190.88	199.63	432.38	422.06
Predictive equation biomass (μg chl *a*.cm^{-2})	$0.0286\,F_{0\ 470nm} - 0.2605$	$0.0274\,F_{0\ 520nm} - 0.1697$	$0.0125\,F_{0\ 645\ nm} - 0.2741$	$0.0128\,F_{0\ 665\ nm} - 0.3039$
r^2	> 0.90	> 0.90	> 0.90	> 0.90

with the *BQ* index, considering the above findings and those of Vázquez-Nion et al. (2018), who after carrying out a calibration for estimating the chl *a* content in biofilms from the F_0 signal at 665 nm, derived from Phyto-PAM measurements, proposed the use of data from this channel (at 665 nm) for expressing the chl *a* content.

3.3. Hyperspectral Imaging Technique

Regarding application of the hyperspectral imaging technique, after the photographs were taken, a 3 cm × 3 cm-area on the surface was selected for recording the reflectance spectra. Reflectance spectra for each pixel were calculated as reported in Section *2.2.4. Hyperspectral Imaging Technique*. Figure 2 shows the mean value of the reflectance of the selected zones in the spectral visible range 450 ~ 700 nm, of the uninoculated (reference) surface (SAM0) and the surfaces inoculated with the different amounts of phototrophs. In the reflectance spectra of this reference granite, it was possible to identify five clearly spectral reflectance signatures:

i) The first signature corresponds to two reflective bands at 460 and 470 nm in which reflectance increased slightly. Different authors (Sabins, 1996; Harris et al., 2005) have assigned these bands to Fe-rich minerals, because iron reflects energy in the red portion of the electromagnetic spectrum and absorbs it in the blue portion. In this granite, Fe is present in biotite grains (6% biotite).

ii) The second signature corresponds to a steep slope between 480 and 635 nm. Harris et al. (2005) assigned this slope to the presence of quartz in monzogranite and quartzite.

Table 3. BQ (%) Computed for Each Inoculated Surface with Different Concentrations by Means of the Hyperspectral Imaging Technique

Biomass concentration (μg chl *a*. cm^{-2})	BQ (%)
1.87	21.19
2.53	31.56
4.41	45.64
5.69	67.36
Predictive equation biomass (μg chla.cm^{-2})	8.9 BQ - 0.05
r^2	0.98

iii) The third reflectance signature is detected at 665 nm, with a weak shoulder.

iv) The fourth signature is reflected by an intense reflectance trough at 670 nm, due to the high absorption of this granite at this wavelength. It was attributed to the presence of quartz (Harris et al., 2005).

v) Slightly higher reflectance was detected for the VNIR wavelength (700 nm). Harris et al. also assigned this increased reflectance to the presence of quartz, because they observed higher reflectance, particularly in the VNIR, in silicate stones with a higher content of quartz (Harris et al., 2005).

The reflectance spectrum exhibited for the reference SAM0 was similar to those obtained for other granites (Pozo-Antonio et al., 2016 a,b).

According to the reflectance spectra for the inoculated surfaces, the initial characteristics of the reference granite at 460 and 470 nm decreased as the amount of biomass increased and were almost totally removed from the spectra in the samples with greater amounts of biomass (5.65 μg chl *a*·cm^{-2}, SAM4). The second reflectance feature of the granite (a steep slope between 480 and 635 nm) was observed in the spectra of the inoculated surfaces. However, it was less intense, as after the addition of the inoculum, the reflectance spectra started to show two new bands at 560 nm (much more intense in the surfaces with higher inoculum concentrations) and at 620 nm, which can be assigned to accessory pigments, such as phycoerytherin and phycocyanin (Ogashawara et al., 2013). Carrère et al. (2004) assigned absorption features at 590 and 635 nm to absorbing pigments such as chlorophyll *c* (Carrère et al., 2004). At 665 ~ 670 nm, intense troughs were registered in the inoculated surfaces, due to the in-vivo absorbance signature for chlorophyll *a* at 675 nm (Hakvoort et al., 1997). Reflectance at this wavelength at which chlorophyll *a* typically

Table 4. r^2 and p-values for the Obtained Results for Each Analytical Technique

BQ (%) and Chl *a*		BQ (%) and F_0		BQ (%) and ΔE^*_{ab}	
r^2	p	r^2	p	r^2	p
0.986	0.0007	0.925	0.0089	0.930	0.0081

* Significance level: $p < 0.05$

absorbs was used by different authors to estimate the concentration of chlorophyll *a* colonizing intertidal sediment by comparison of the reflectance at this wavelength with that registered at wavelengths without absorption attributable to chl *a*, mainly in the 720 ~ 800 nm range (Carrère et al., 2004; Chennu et al., 2013). The reflectance spectra of the colonized surfaces showed an approximately linear trend and higher intensity than that registered on the reference granite spectrum (SAM0) at VNIR wavelength range (~ 700 nm). Barillé et al. attributed this linear trend to the combined effects of absorption and scattering by the sediment-seawater matrix (Barillé et al., 2011). This property therefore seems to be related to the presence of features containing water because it is absorbed more strongly at a longer wavelength and near-infrared radiations than at visible wavelengths (Vincikováet al. 2015). In water bodies, Vincinková et al. (2015) observed distinct peaks at green, red and NIR wavelengths with the reflectance values of 1 ~ 6% in the green region at around 510 nm, 2 ~ 4% at around 650 nm (red) and between 4 and 12% at around 700 nm. These higher reflectance features at around 700 nm were used by other researchers to detect algae colonies in inland waters (Kudela et al., 2015). Other authors found that the increased reflectance intensity of the peak at about 700 nm (near-infrared peak) is related to the increase in chlorophyll *a* concentration
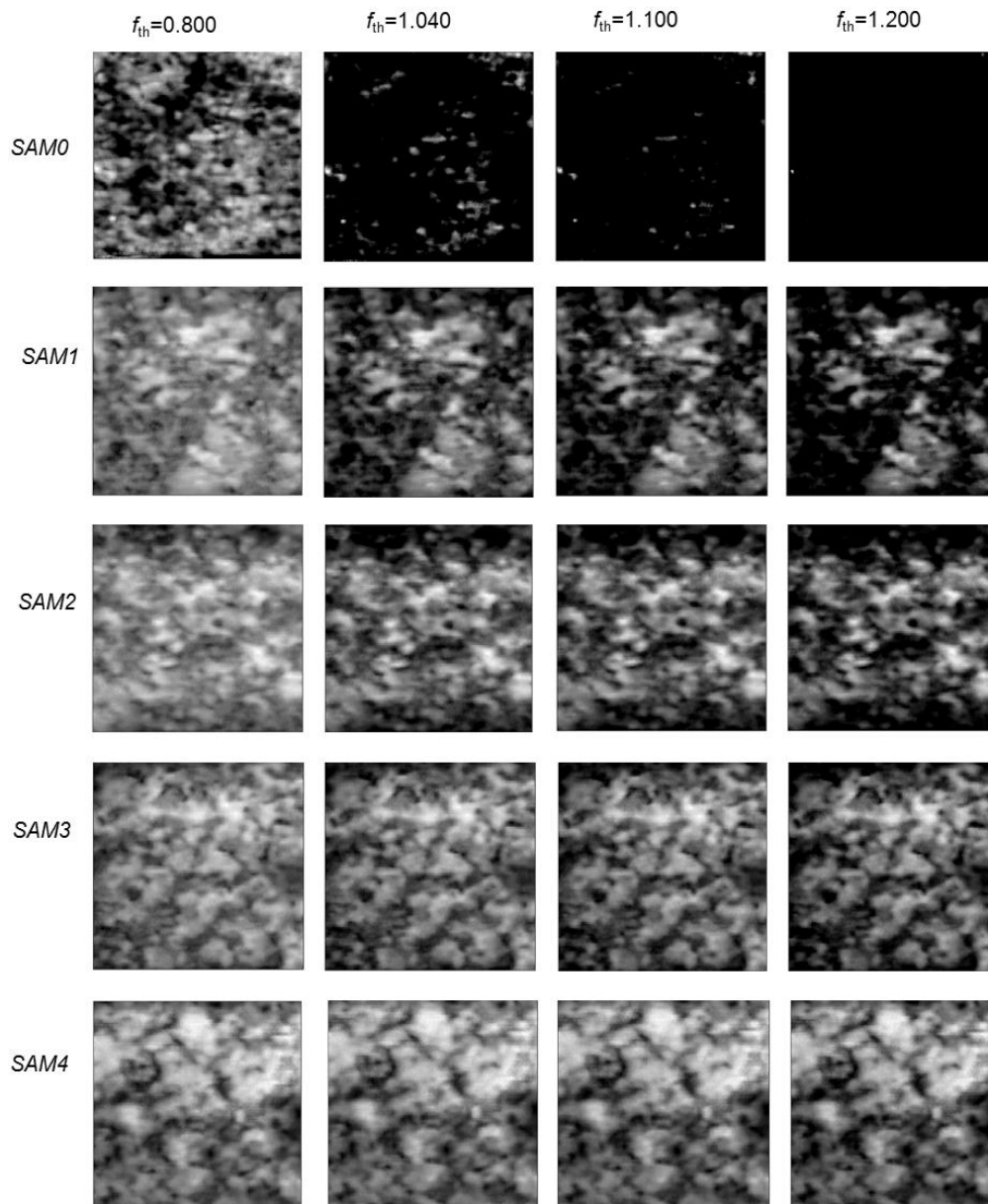

Figure 5. For each row, reference surface without inoculum (SAM0), and inoculated with dry weight biomass 0.05 (SAM1), 0.10 (SAM2), 0.15 (SAM3) and 0.20 mg·cm^{-2} (SAM4). The columns correspond to the pixel distribution maps with $f_{GR} > f_{th}$ for values of f_{th} = 0.800, 1.040, 1.100 and 1.200.

(Gitelson et al. 1999). The steepness and clarity of these features are also affected by the optical scattering properties of the substrate. The chl *a* absorption probably masks this weak effect observed on uninoculated granite.

In comparison to the reference granite (SAM0), all the variations registered on the reflectance of the inoculated surfaces are related to the biological growth on the surfaces. Gitelson et al. found similar reflectance features in different freshwater algal phyla *(Chlorophyta, Cyanophyta, Bacillariophyta* and *Pyrrophyta)*: a depression between 440 and 500 nm, a conspicuous trough at around 670 nm and prominent peaks centred at around 570 and 700 nm (Gitelson et al. 1999). The intensity of reflectance decreased with increasing concentration of biomass (Figure 2).

3.4. Hyperspectral Image Analysis: *BQ* Index Computation and Correlations with Δ*E**$_{ab}$ and *F*$_0$

Considering this specific case, in the areas colonized by algae, the reflectance spectrum shows higher values in the green band, *G* (550 ± 10 nm), than in the red range, *R* (670 ± 10 nm) (Figure 2). Conversely to the colonized areas, the reference granite exhibits higher reflectance in the red area. Note that in the current study, reflectance spectra were obtained in the visible region (450 ~ 700 nm); thus, conversely to other authors, the reflectance wavelengths used to compute the *BQ* index could not be taken in the NIR region (Carrère et al., 2004, Chennu et al., 2013). Optimization of the application of this hyperspectral system was therefore carried out. As result, a green-red factor, *f*$_{GR}$, is defined as *f*$_{GR}$ = *R*$_G$/*R*$_R$, in which *R*$_G$ was the reflectance value assigned to the green region (540 to 560 nm) and *R*$_R$ was the reflectance value for the red area (660 to 680 nm) of the spectrum of each pixel.

Figure 6. Linear correlation between *BQ* (%) and (a) Δ*E**$_{ab}$ and (b) *F*$_0$.

$$f_{GR} = \frac{R_G}{R_R} = \frac{\int_{540nm}^{560nm} R(\lambda)d\lambda}{\int_{660nm}^{680nm} R(\lambda)d\lambda} \qquad (6)$$

The digital photographs and images corresponding to the reflectance of the *R* and *G* bands and the quotient *f*$_{GR}$ are shown in Figure 3. As the concentration of the inoculum increased, the difference in intensity between the image of the *R* band and the *G* band and therefore the *f*$_{GR}$ increased. The value of *f*$_{GR}$ will be greater in the pixels in which the concentration of algae is greater, regardless of their corresponding mineral. After capturing the reflectance spectra, the biofilm quantification (*BQ*) index was computed as follows:

$$BQ = \begin{cases} \log(f_{GR}) - \log(f_{th}) & if & f_{GR} > f_{th} \\ 0 & if & f_{GR} \leq f_{th} \end{cases} \qquad (7)$$

The *BQ* was computed for different threshold *f*$_{th}$ values (Figure 4). The optimal value of the threshold was determined by analysing the correlation coefficient, *r*^{2}, and the root mean square error (*r.m.s.*) for the linear fit of *BQ* relative to the amount of chlorophyll *a* (Figure 4) for different values of *f*$_{th}$ between 0.500 and 1.500. As shown in Figure 4, the highest correlation coefficient and the lowest mean square error correspond to *f*$_{th}$=1.040.

Consequently, considering a *f*$_{th}$ of 1.040, the *BQ* index for each colonized surface was computed (Table 3). The statistical relationships between the BQ and the biomass concentration are also shown in Table 3. *BQ* increased with the inoculum concentration (Figure 3), with a coefficient of determination *r*^{2} of 0.98. Thus, the *BQ* index provides information about the amount of colonized surface and also the amount of biomass.

According to the correlations between the results of the different analytical techniques, the *BQ* index was linearly correlated with chl *a*, *F*$_0$ and Δ*E**$_{ab}$; *r*^{2} was higher than 0.92 (Figure 6 and Table 4). Thus, the proposed *BQ* index computed from the reflectance spectra in the visible range (450 ~ 700 nm) is as useful as chl *a*, *F*$_0$ and Δ*E**$_{ab}$ for quantifying phototrophic colonization on granitic surfaces.

4. Conclusions and Final Remarks

In this study, a hyperspectral imaging technique involving computation of the *BQ* index from the reflectance spectra in the visible range 450 ~ 700 nm is proposed as a reliable tool for quantifying the green fouling on chromatically and texturally heterogeneous granitic stones. The suitability of this hyperspectral camera has been verified by other commonly used techniques for quantifying biological colonization, i.e. chemical extraction of chl *a*, colour spectrophotometry and PAM-fluorometry. Although the results showed that the proposed *BQ* index is as useful as chl *a*, *F*$_0$ and Δ*E**$_{ab}$ for quantifying pho-
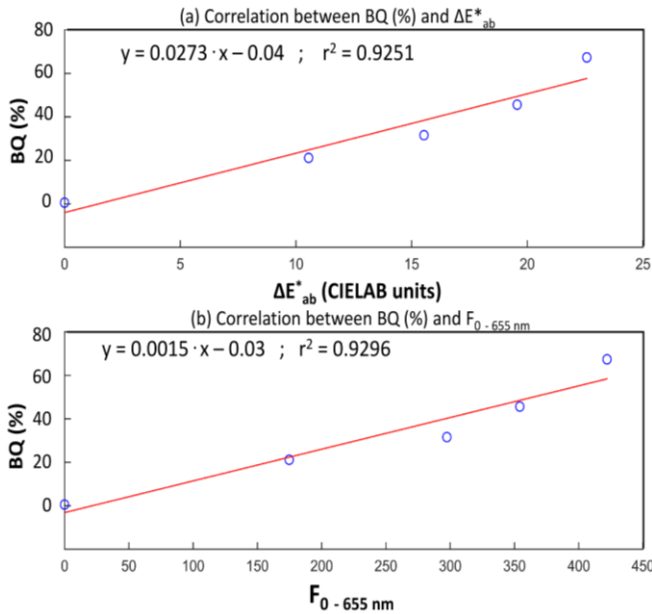
totrophic colonization on a granitic surface, the former shows some important advantages:

(1) Hyperspectral imaging makes it possible to measure large surfaces (façades) while the other techniques take longer time and, in some cases, require the use of scaffolding.

(2) Hyperspectral imaging provides information about the distribution of the biocolonization on the surface by producing maps of biomass distribution, while the other techniques produce an average of several point measurements without identifying the exact distribution.

(3) The *BQ* index enables quantification of the cover on granite surfaces by phototrophs thus making it possible to monitor the phototrophic colonization. Further studies should be conducted in order to evaluate the potential monitoring of biological growth by the hyperspectral technique, by measuring biofilm growth in periods longer than 21 days.

Taking into account that the hyperspectral technique allowed the non-destructive, *in situ* and on site determination of the distribution of the biological colonization and subsequent quantification on granite by computation of the *BQ* index, the method seems to be a promising tool of monitoring phototrophic colonization on the built cultural heritage.

References

Barillé, L., Mouget, J.L., Méléder, V., Rosa, P., and Jesus, B. (2011). Spectral response of benthic diatoms with different sediment backgrounds. *Remote Sens. Environ.,* 115(4), 1034-1042. https://doi.org/10.1016/j.rse.2010.12.008

Berns, R.S. (2000). *Billmeyer and Saltzman's Principles of Color Technology, 3rd edition,* New York, Wiley.

Carrère, V., Spilont, N., and Davoult, D. (2004). Comparison of simple techniques for estimating chlorophyll *a* concentration in the intertidal zone using high spectral-resolution field-spectrometer data. *Mar. Ecol. Prog. Ser.,* 274, 31-40. https://doi.org/10.3354/meps274031

Chennu, A., Färber, P., Volkenborn, N., Al-Najjar, M.A.A., Janssen, F., de Beer, D., and Polerecky, L. (2013). Hyperspectral imaging of the microscale distribution and dynamics of microphytobenthos in intertidal sediments. *Limnol. Oceanogr.,* 11(10), 511-528. https://doi.org/10.4319/lom.2013.11.511

Colorimetry CIE Central Bureau. (1986). *CIE Publication 15-2,* Vienna.

Crispim, C.A. and Gaylarde, C.C. (2005). Cyanobacteria and biodeterioration of cultural heritage, A review. *Microb. Ecol.,* 49(1), 1-9. https://doi.org/10.1007/s00248-003-1052-5

Cutler, N.A., Viles, H.A., Ahmad, S., McCabe, S., and Smith, B.J. (2013). Algal 'greening' and the conservation of stone heritage

structures. *Sci. Total Environ.,* 442(1), 152-164. https://doi.org /10.1016/j.scitotenv.2012.10.050

De Muynck, W., Ramirez, A.M., and De Belie, N., Verstraete, W. (2009). Evaluation of strategies to prevent algal fouling on white architectural and cellular concrete. *Int. Biodeterior. Biodegrad.,* 63 (6), 679-689. https://doi.org/10.1016/j.ibiod.2009.04.007

Eggert, A., Häubner, N., Klausch, S., Karsten, U., and Schumann, R. (2006). Quantification of algal biofilms colonising building materials: chlorophyll-a measured by PAM fluorometry as a biomass parameter. *Biofouling,* 22(2), 79-90. https://doi.org/10.1080/08927010600579090

Eismann, M.T. (2012). *Hyperspectral Remote Sensing,* pp.748. https://doi.org/10.1117/3.899758

EN 1936-1999 (1999). *Natural Stone Test Method-Determination of Real Density and Apparent Density, and of Total and Open Porosity,* European Committee for Standardization (CEN), Belgium

Eyssautier-Chuine, S, Vaillant-Gaveau, N, Gommeaux, M, Thomachot-Schneider, C, Pleck, J and Fronteau, G (2015). Efficacy of different chemical mixtures against green algal growth on limestone: a case study with Chlorella vulgaris. *Int. Biodeterior. Biodegrad.,* 103, 59-68. https://doi.org/10.1016/j.i biod.2015.02.021

Fernández-Silva, I., Sanmartín, P., Silva, B., Moldes, A., and Prieto, B. (2011). Quantification of phototrophic biomass on rocks: optimization of chlorophyll-*a* extraction by response surface methodology. *J. Ind. Microbiol. Biotechnol.,* 38, 179-188. https://doi.org/10.1007/s10295-010-0843-1

Gitelson, A.A., Schalles, J.F., Rundquist, D.C., Schiebe, F.R., and Yacobi, Y.Z. (1999). Comparative reflectance properties of algal cultures with manipulated densities. *J. Appl. Phycol.,* 11(4), 345-354. https://doi.org/10.1023/A:1008143902418

Gladis, F. and Schumann, R. (2011). Influence of material properties and photocatalysis on phototrophic growth in multi-year roof weathering. *Int. Biodeterior. Biodegrad.,* 65(1), 36-44. https://doi.org/10.1016/ j.ibiod.2010.05.014

Goetz, A.F.H. (2009). Three decades of hyperspectral remote sensing of the Earth: A personal view. *Remote Sens. Environ.,* 113(1), S5-S16. https://doi.org/10.1016/j.rse.2007.12.014

Gorbushina, A.A. (2007). Life on the rocks. *Environ. Microbiol.,* 9(7), 1613-1631. https://doi.org/10.1111/j.1462-2920.2007.013 01.x

Gowen, A.A., Feng, Y., Gaston, E., and Valdramidis, V. (2015). Recent applications of hyperspectral imaging in microbiology. *Talanta,* 137(5), 43-54. https://doi.org/10.1016/j.talanta.2015.0 1.012

Hakvoort, H., Heymann, K., Stein, C., and Murphy. D. (1997). In situ optical measurements of sediment type and phytobenthos of tidal flats: a basis for imaging remote sensing spectroscopy. *Ocean Dyn.,* 49(2-3), 367-373. https://doi.org/10.1007/BF02 764045

Harris, J.R., Rogge, D., Hitchcock, R., Ijewliw, O., and Wright D. (2005). Mapping lithology in Canada's Arctic: application of hyperspectral data using the minimum noise fraction transforma- tion and matched filtering, *Can. J. Earth Sci.,* 42(12), 2173-2193. https://doi.org/10.1139/e05-064

Kudela, R.M., Palacios, S.L., Austerberry, D.C., Accorsi, E.K., Guild, L.S., and Torres-Perez, J. (2015). Application of hyperspectral remote sensing to cyanobacterial blooms in inland waters. *Remote Sens. Environ.,* 167, 196-205. https://doi.org/10.1016/j.rse.2015.01. 025

López, A.J., Ramil, A., Pozo-Antonio, J.S., Fiorucci, M.P., and Rivas T. (2007). Automatic identification of rock-forming minerals in granite using laboratory scale hyperspectral reflec- tance imaging and artificial neural networks. *J. Nondestr. Eval.,* 36(3). https://doi.org/10.1007/s10921-017-0431-7

Ogashawara, I., Misra, D.R., Mishra, S., Curtarelli, M.P., and Stech, J.L. (2013). A performance review of reflectance based algorithms for predicting phycocyanin concentrations in inland waters. *Re-*

mote Sens., 5(10), 4774-4798. https://doi.org/10.3390/rs5104774

Ortega-Calvo, J.J., Hernández-Marine, M., and Saiz-Jimenez, C. (1991a). Biodeterioration of buildings materials by cyanobac- teria and algae. *Int. Biodeterior.,* 28(1-4), 165-186. https://doi.org/10. 1016/0265-3036(91)90041-O

Ortega-Calvo, J.J., Hernández-Marine, M., and Saiz-Jimenez, C. (1991b). Mechanical deterioration of building stones by cyano-bacteria and algae. *Biodeterioration and Biodegradation,* KW. Rossmoore, Elsevier, London, pp. 392-394

Pozo-Antonio, J.S., Fiorucci, M.P., Ramil, A., López, A.J., and Rivas, T. (2015). Evaluation of the effectiveness of laser crust removal on granites by means of hyperspectral imaging techniques. *Appl. Surf. Sci.,* 347(30), 832-838. https://doi.org/10.1016/j.apsusc.2015.04.182

Pozo-Antonio, J.S., Fiorucci, M.P., Rivas, T., López, A.J., Ramil, A., and Barral, D. (2016a). Suitability of hyperspectral imaging tech-nique to evaluate the effectiveness of the cleaning of a crustose lichen developed on granite. *Appl. Phys. A,* 122(2), 1-9. https://doi.org/10.1007/s00339-016-9634-5

Pozo-Antonio, J.S., Ramil, A., Fiorucci, M.P., López, A.J., and Rivas, T. (2016b). The use of hyperspectral imaging technique to detect the most suitable graffiti-cleaning procedure. *Color Res. Appl.,* 41(3). https://doi.org/10.1002/col.22032

Prieto, B., Rivas, T., and Silva, B. (2002). Rapid quantification of phototrophic microorganisms and their physiological state through their colour. *Biofouling,* 18(3), 229-36. https://doi.org/10.1080/08 927010290014917

Prieto, B., Silva, B., Aira, N., and Laiz, L. (2005). Induction of biofilms on quartz surfaces as a means of reducing the visual im-pact of quartz quarries. *Biofouling,* 21(5-6), 237-246. https://doi.org/10.1080/08927010500421294

Prieto, B., Sanmartín, P., Aira, N., and Silva, B. (2010a). Color of cyanobacteria: some methodological aspects. *Appl Optics,* 49(1), 2022-2029. https://doi.org/10.1364/AO.49.002022

Prieto, B., Sanmartín, P., Silva, B., and Martínez-Verdú, F. (2010b). Measuring de the color of granite rocks. A proposed procedure. *Color Res. Appl.,* 35(5), 368-375. https://doi.org/10.1002/col.20579

Ramirez, M., Hernandez-Marine, M., Novelo, E., and Roldán, M. (2010). Cyanobacteria-containing biofilms from a Mayan mon-ument in Palenque, Mexico. *Biofouling,* 26(4), 399-409. https://doi.org/10.1080/08927011003660404

Sabins, F. (1996). *Remote Sensing Principles and Interpretation,* 3rd edition, W.F. Freeman and Co., New York, N.Y.

Sanmartín, P., Aira, N., Devesa-Rey, R., Silva, B., and Prieto, B. (2010). Relationship between color and pigment production in two stone biofilm-forming cyanobacteria (Nostoc sp PCC 9104 and Nostoc sp PCC 9025). *Biofouling,* 26(5), 499-509. https://doi.org/10.1080/08927011003774221

Sanmartín, P., Villa, F., Silva, B., Cappitelli, F., and Prieto, B. (2011).

Color measurements as a reliable method for estimating chloro-phyll degradation to phaeopigments. *Biodegradation,* 22(4), 763-771. https://doi.org/10.1007/s10532-010-9402-8

Sanmartín, P., Vázquez-Nion, D., Silva, B., and Prieto, B. (2012). Spectrophotometric color measurement for early detection and mon-itoring of greening on granite buildings. *Biofouling,* 28(3), 329-338. https://doi.org/10.1080/08927014.2012.673220

Scheerer, S., Ortega-Morales, O., and Gaylarde, C. (2009). Microbial deterioration of stone monuments-an updated overview. *Adv. Appl. Microbiol.,* 66, 97-139. https://doi.org/10.1016/S0065-2164(08)00 805-8

van der Meer, F.D., van der Werff, H.M.A., van Ruitenbeek, F.J.A., Hecker, C.A., Bakker, W.H., Noomen, M.F., van der Meijde, M., Carranza, E.J.M., de Smeth, J.B., and Woldai, T. (2012). Multi-and hyperspectral geologic remote sensing: A review. *Int. J. Appl. Earth Obs. Geoinf.,* 14(1), 112-128. https://doi.org/10.1016/j.jag. 2011.08.002

Vázquez-Nion, D., Rodríguez-Castro, J., López-Rodríguez, M.C., Fernández-Silva, I., and Prieto, B. (2016). Subaerial biofilms on granitic historic buildings: microbial diversity and development of phototrophic multi-species cultures. *Biofouling,* 32(6), 657-669. https://doi.org/10.1080/0892701 4.2016.1183121

Vázquez-Nion, D., Silva, B., and Prieto, B. (2018). Influence of the properties of granitic rocks on their bioreceptivity to subaerial pho-totrophic biofilms. *Sci. Total. Environ.,* 610-611(1), 44-54. https://doi.org/10.1016/j.scitotenv.2017.0 8.015

Vicente, M.A., Delgado Rodrigues, J., and Acevedo, J., (1996). *Degradation and Conservation of Granitic Rocks in Monument,* Protection and Conservation of the European Cultural Heritage Research Report No. 5, European Commission, Brussels, Belgium.

Villa, F., Stewart. P., Klapper. I., Jacob. J., and Cappitelli. F. (2016). Subaerial biofilms on outdoor stone monuments: changing the perspective towards an ecological framework, *BioScience,* 66(4), 285-294. https://doi.org/10.1093/biosci/bi w006

Vincinková, H., Hanus, J., and Pechar, L. (2015). Spectral reflectance is a reliable water-quality estimator for small, highly turbid wet-lands. *Wetlands Ecol. Manage.,* 23(5), 933-946. https://doi.org/10.1007/ s11273-015-9431-5

Völz, H.G. (2001). *Industrial Color Testing,* Weinheim: Wiley- VCH. https://doi.org/10.1002/3527600485

von Werder, J. and Venzmer, H. (2015). Černý R. Application of fluorometric and numerical analysis for assessing the algal resis-tance of external thermal insulation composite systems. *J. Build. Phys.,* 38(4), 290-316. https://doi.org/10.1177/1744259113506073

Wellburn, A.R. (1994). The spectral determination of chlorophylls a and b, as well as total carotenoids, using various solvents with spectrophotometers of different resolution. *J. Plant Physiol.,* 144 (3), 307-313. https://doi.org/ 10.1016/S0176-1617(11)81192-2